International Journal of Signal Processing, Image Processing and Pattern Recognition
Vol.7, No.3 (2014), pp.305-316
http://dx.doi.org/10.14257/ijsip.2014.7.3.25

Lossless Compression of Hyperspectral Images Using Three-Stage Prediction with Adaptive Search Threshold

Changguo Li[1,2,*] and Ke Guo[1]

[1]*College of Geophysics, Chengdu University of Technology, Chengdu, Sichuan, 610059, China*
[2]*College of Fundamental Education, Sichuan Normal University, Chengdu, Sichuan, 610068, China*
389224879@qq.com

Abstract

We propose a new lossless compression algorithm for hyper spectral images based on the third-order interband predictor and the backward pixel search scheme (IP3-BPS). Specifically, we propose an adaptive search threshold algorithm and a bi-directional pixel search scheme. The resulting algorithm takes the bi-directional pixel search and the backward pixel search with adaptive search threshold as the last two predictors; its performance evaluation on Airborne Visible/Infrared Imaging Spectrometer (AVIRIS) 1997 images shows that it outperforms the original IP3-BPS algorithm, at lower computational complexity level.

Keywords: *Hyperspectral images, Image compression, Lossless compression, Adaptive arithmetic coding, Adaptive search threshold*

1. Introduction

Hyperspectral images have recently received a lot of attention, as their high spectral resolution allows one to distinguish different materials, facilitating several image analysis tasks, particularly image classification. However, hyperspectral data sets have very large size, making acquisition, storage, and transmission of these data problematic. For example, a scene data cube recorded by the National Aeronautics and Space Administration Jet Propulsion Laboratory Airborne Visible/Infrared Imaging Spectrometer (AVIRIS) contains 224 bands of 512×614 sized images. The data storage requirement for one scene only reaches 140 MB.

A possible solution lies in the adoption of compression techniques. The accuracy of the hyperspectral data analysis depends on the quality of the hyperspectral data. The accuracy of the data analysis might be of interest to different academic, defense, and commercial applications. Thus, lossy data compression reducing data quality might not be a proper solution for all data reduction purposes. Lossless data compression could be used instead if the quality of the data is a concern. Our focus in this paper is on lossless compression.

In this paper, we propose an effective technique for lossless compression of hyperspectral data, which uses IP3-BPS as spatial-spectral compression engine. Specifically, we propose an efficient adaptive search threshold algorithm and a modified spatial-spectral predictor, suitable for lossless compression of hyperspectral data, which is able to capture most of the correlation by performing twice pixel search in current band. Experimental results on AVIRIS scenes show that the proposed technique outperforms IP3-BPS, as well as other state-of-the-art techniques, with very limited memory resources. The rest of this paper is organized as follows. Section II reviews previous methods. In Section III, the ground work for the

ISSN: 2005-4254 IJSIP

proposed method is prepared by presenting a brief sketch of IP3-BPS. Sections IV and V describe the adaptive search threshold algorithm, the bi-directional pixel search scheme, respectively. The whole compression method and experimental results are given in Section VI. Section VII concludes this paper.

2. Review of Previous Methods

Compression relies on statistical structure in the data. In hyperspectral images, there are basically two types of correlation available. One is spatial correlation in adjacent pixels in the same band, and the other is spectral correlation in pixels between adjacent bands. The spectral correlation is much stronger than the spatial correlation, and it must be utilized for maximal compression performance. Usually, lossless compression of hyperspectral data is performed by using prediction-based approaches because transform-based and vector-quantization-based methods have not been able to achieve state-of-the-art results.

Predictive coding approaches usually employ spatial, spectral, or hybrid predictors to decorrelate the image, followed by entropy coders. Wu and Memon [1] extend the CALIC algorithm [3] from 2-D to 3-D. The algorithm switches between two modes, intraband and interband prediction, based on the correlation coefficient. The resulting residual is then coded using context-based arithmetic codes. Magli, *et al.*, propose a modified 3-D CALIC (M-CALIC) [2] for lossless and near-lossless compression. Rather than switching between interband and intraband modes, as in 3-D CALIC, M-CALIC works with a full interband and a universal spectral predictor. It refines the prediction models and optimizes parameters of context coding to achieve a good coding performance. Tate shows that the band order could be rearranged and optimized for better interband prediction, and therefore, better compression ratios could be achieved [4]. Recently, Zhang and Liu proposed a two-step adaptive spectral-band-reordering algorithm [5]. First, the bands are classified into groups based on the correlation factor of adjacent bands, and then, a reordering algorithm based on the Prim algorithm is applied to each group. A prediction method called ABPCNEF is proposed to take advantage of the similarity of structure and pixel relationship between two neighboring spectral bands and the residual is coded using adaptive arithmetic coding. However, in this paper, all the experiments are performed using natural ordering of the bands to facilitate comparisons to the other methods in the literature.

Rizzo, *et al.*, presented an adaptive least-squares optimized prediction technique called spectrum-oriented least squares (SLSQ) [6]. The predictor is optimized for each pixel and each band in a causal neighborhood of the current pixel. SLSQ-HEU uses an offline heuristic to select between intraband and an intraband compression mode. They also presented an optimal method for inter/intra mode selection called SLSQ-OPT. Kiely and Klimesh proposed a fast lossless algorithm (TSP-W2) [7] focusing on onboard compression, which employs the previous band for prediction and adapts the predictor coefficients using recursive estimation.

The rationale of a purely spectral prediction performed on pre-classified data has led to the development of the crisp and fuzzy adaptive spectral predictors, referred to as Spectral-Relaxation Labeled Prediction (S-RLP) and Spectral-Fuzzy Matching Pursuits (S-FMP) [9]. The former is a modified version of 3-D RLP [8], with a hard pre-classified prediction along the spectral direction only. The latter is analogous except for the pre-classified prediction, which is soft. The two methods slightly differ in performances, better for S-FMP, and in computational complexity, lower for S-RLP.

In a recent publication [10], Mielikainen and Toivanen proposed a clustered differential pulse-code modulation (C-DPCM) scheme, where the spectral bands of the image are clustered then filtered using an optimum linear filter for each cluster. The output of the filters is encoded using an adaptive entropy coder. In their follow-up work, which they called

lookup Table (LUT) method [11], the pixel that is nearest and equal to the pixel colocated with the one to be predicted in the previous band is taken as the prediction. The locally averaged interband scaling (LAIS)-LUT method [12] enhanced the LUT method. First, the method computes a LAIS estimate by scaling the pixel collocated in the previous band. The scaling factor is an average of ratios between three neighboring causal pixels in the current and previous bands. Two LUTs are used, each of which is similar to the one used in the LUT method. The second LUT is updated with the past entries of the first LUT. The predictor returned by the LUT that is the closest one to the LAIS estimate is chosen as the predictor for the current pixel. If the LUTs return no match, the LAIS estimate is used as the predictor. The addresses of the two LUTs in the LAIS-LUT method may be quantized to yield a closer, and hence more fitting, nearest neighbor (NN) and to improve the selection between the LUTs based on the LAIS reference. This method, known as LAIS-QLUT [13], employs either a heuristic or an exhaustive strategy to determine the quantization step size, which may vary from one band to another. Eventually, the LUT method was further extended to multiband and multiLUT [14]. That is, M LUTs are defined on each of the N previous bands, from which prediction is calculated. The decision among one of the M•N possible prediction values is based on the closeness of the values contained in the LUTs to an advanced prediction carried out from the values in the same N previous bands. Such a prediction is provided by either of S-RLP or S-FMP.

3. IP3-BPS

As we all know, the essence of hyperspectral images compression is to reduce their redundancies. For calibration-induced hyperspectral images, besides spatial and spectral redundancies, they have calibration-induced data redundancy [7]. In [15], Lin and Hwang proposed a two-stage prediction method based on these three redundancies, named IP3-BPS, consisting of a third-order interband predictor and a backward pixel search scheme, which outperforms all other schemes under comparison in this category. First, for interband prediction, the third-order predictor (IP3) is adopted and has the following prediction formula:

$$\hat{y} = \alpha(v - m_v) + \beta(w - m_w) + \gamma(x - m_x) + m_y \quad (1)$$

Where "x", "w", and "v" denote the pixels colocated with the current pixel in three previuos bands and "m" stands for the expectation value of a random variable. Prediction coefficients α, β, *and* γ can be derived by solving a Wiener-Hopf equation

$$\begin{bmatrix} \sigma_v^2 & \sigma_{wv} & \sigma_{xv} \\ \sigma_{wv} & \sigma_w^2 & \sigma_{xw} \\ \sigma_{xv} & \sigma_{xw} & \sigma_x^2 \end{bmatrix} \begin{bmatrix} \alpha \\ \beta \\ \gamma \end{bmatrix} = \begin{bmatrix} \sigma_{yv} \\ \sigma_{yw} \\ \sigma_{yx} \end{bmatrix} \quad (2)$$

Refer to the context window definition in Figure 1; the statistical parameters can be approximated as

$$\sigma_x^2 = E\{x^2\} - m_x^2 = \frac{1}{M^2}\left(M\sum_{i=1}^{M} x_i^2 - \left(\sum_{i=1}^{M} x_i\right)^2\right) \quad (3)$$

$$\sigma_{wy} = E\{wy\} - m_w m_y = \frac{1}{M^2}\left(M\sum_{i=1}^{M} w_i y_i - \sum_{i=1}^{M} w_i \sum_{i=1}^{M} y_i\right) \quad (4)$$

Secondly, the backward pixel search (BPS) scheme as the Stage-2 predictor is employed specifically for images with pronounced calibration-inducaed artifacts. The prediction obtained from the first stage is treated as a prediction reference P_{ref} . The causal pixels in the current band are searched, and the one with a pixel value that is closest to P_{ref} is selected as the final prediction. In BPS algorithm, the band scaling factors used to convert from raw digital number (DN) values to radiance values are used as the upper bound in searching for the optimal threshold value for each band.

	y_{32}	y_{30}	y_{28}	y_{27}	y_{29}	y_{31}
y_{26}	y_{22}	y_{20}	y_{18}	y_{17}	y_{19}	y_{21}
y_{25}	y_{16}	y_{13}	y_9	y_7	y_6	y_{10}
y_{24}	y_{15}	y_{12}	y_8	y_3	y_2	y_4
y_{23}	y_{14}	y_{11}	y_5	y_1	y	

Figure 1. Definition of Context Window for Interband Prediction

4. Adaptive Search Threshold

In general, the compression performance is not proportional to the computational complexity for most of lossless compression algorithms, and IP3-BPS is no exception. However, it found that the threshod method can speed up the search in BPS algorithm, and as the value of threshold is increased, the search gets faster. Thus, in the case of specified compression performance, we propose an adaptive search threshold (AST) algorithm in order to further accelerate the search. The adaptive search threshold is defined as

$$T_k = \frac{\sum_{i=1}^{M}\sum_{j=1}^{N}\left|\hat{I}(k,i,j) - I(k,i,j)\right|}{MN} \quad \textbf{(5)}$$

Where $\hat{I}(k,i,j)$ is the stage-1 prediction of pixel $I(k,i,j)$, M and N are the width and height of each image. Experiments show that T_k can be an effective comprehensive assessment of intraband pixel threshold values. Figure 2 shows the adaptive search threshold values of four sequences of AVIRIS'97; they all exhibit very similar profiles. Thus, we may apply the adaptive search threshold of one sequence to compress all hyperspectral images.

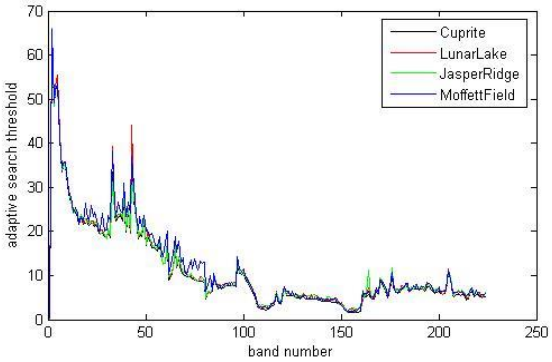

Figure 2. Adaptive Search Threshold for the AVIRIS'97 Hyperspectral Images

5. Bi-directional Pixel Search

5.1. Adaptive Spectral Band Grouping

We define the spectral correlation factor as $C_k(t)$, which is calculated by

$$C_k(t) = \frac{\sum_{i=1}^{M}\sum_{j=1}^{N}(I(k,i,j)-\bar{I}_k)(I(k+t,i,j)-\bar{I}_{k+t})}{\sqrt{\sum_{i=1}^{M}\sum_{j=1}^{N}(I(k,i,j)-\bar{I}_k)^2\sum_{i=1}^{M}\sum_{j=1}^{N}(I(k+t,i,j)-\bar{I}_{k+t})^2}} \quad (6)$$

Where $I(k,i,j)$ and $\bar{I}_k$ are the pixel value at location (i, j) and mean pixel value of band k, respectively.

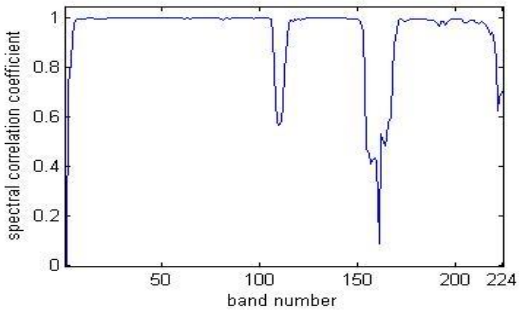

Figure 3. Correlation Coefficient Curves of Adjacent Bands of Cuprite Data

From Figure 3, we can find that the spectral correlations are not always high. For some bands, the spectral correlations are very weak, in which case only interband prediction IP3-BPS is used and could get good performances. At the same time, the computational time can be slightly decreased. Thus, there is need to group the spectral bands. The simple adaptive spectral band grouping we used is shown in Figure 4, by performing one step. Namely: 1) calculate the spectral band correlation factors $C_k(1)$ for all the bands. If $C_k(1) > 0.9$, the two adjacent bands k and (k+1) belong to the same group n; otherwise, they belong to different groups n and (n+1).

After execution of the simple adaptive spectral band grouping algorithm, the bands that need further carrying out the bi-directional pixel search algorithm are known.

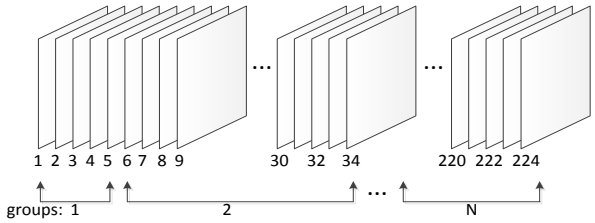

Figure 4. Adaptive Spectral Band Grouping

5.2. Bi-directional Pixel Search Algorithm

From section III, we can see that the backward pixel search scheme uses mainly calibration-induced data correlation to further compress image data. And in the pixel search process, it takes the band scaling factors as the upper bound, which can speed up the search and improve the compression performance. However, by further analysis of the BPS algorithm, it can be found that taking the band scaling factor as the upper bound of all pixel searches in the corresponding band can't ensure that the searched pixel value is local optimization. Namely, pixel with smaller value may be existed in the search scope of ten pixel rows. Thus, we propose a bi-directional pixel search scheme based on calibration-induced data redundancy for further compressing hyperspectral images.

The block diagram of the proposed bi-directional pixel search scheme is shown in Figure 5. Here, spectral bands k1-kn belongs to a group, which has high correlation bands ($C_k(1) > 0.9$). For the first and final bands in the group, if the group is the first group in the spectral band sequence, only intraband prediction JPEG-LS [16] is applied to the two bands; otherwise, only JPEG-LS is applied to the final band. For other bands in the group, after execution of IP3 and BPS predictors, an additional predictor, bi-directional pixel search, is adopted. It uses the previous and final bands as reference bands. For example, band K2 is predicted by bands k1 and kn; bands k2 and kn are used to predict band k3 (note that in the next text, the prediction of the current pixel is discussed in this group, in which the bands have high correlation).

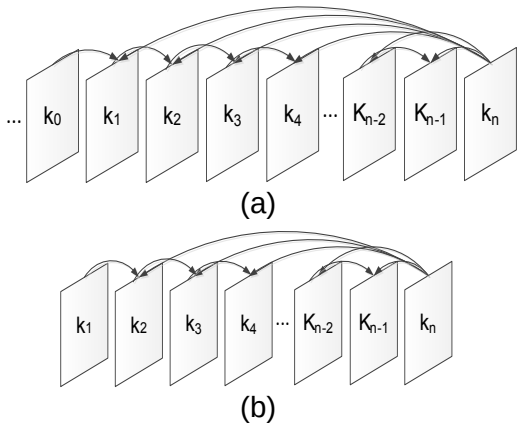

Figure 5. Flowcharts of the Proposed Bi-Directional Pixel Search Algorithm in (a) the First Group and (b) the other Groups

In the prediction process, we define the current pixel as $f(k, m, n)$ (kth band, mth row, and nth column). A prediction of the current pixel $f(k, m, n)$ using all the causal pixels, which are in the previous, current and final bands, is made. First, a pixel value equal to $f(k-1, m, n)$ and $f(k_{final}, m, n)$ is searched in the previous and final bands, respectively. If equal valued pixels $f(k-1, m'_1, n'_1)$, $f(k_{final}, m''_1, n''_1)$, $f(k-1, m'_2, n'_2)$, $f(k_{final}, m''_2, n''_2)$, …, $f(k-1, m'_t, n'_t)$, $f(k_{final}, m''_t, n''_t)$ ($1 \le t \le M \cdot N$, where M is the number of the rows, N is the number of the columns) are found. The decision among one of the possible prediction values $f(k, m'_1, n'_1)$, $f(k, m''_1, n''_1)$, $f(k, m'_2, n'_2)$, $f(k, m''_2, n''_2)$, …, $f(k, m'_t, n'_t)$, $f(k, m''_t, n''_t)$ is based on the closeness of the values to the prediction reference value P_{ref}. Otherwise, the estimated pixel value is equal to the prediction reference value P_{ref}. The whole search is performed in the reverse scanning order. Naturally, these guarantee that the final prediction value is rarely more than the prediction reference value P_{ref}.

In order to speed up the search, two LUTs for each of the previous and final spectral bands are utilized and updated, analogously to [11, 12, 14] in the following way:

Let $L_i^{(k)}[\cdot]$ (i=1, 2, 3, 4) indicate the set of four LUTs used for prediction of band k. All LUTs are of length $f_{\max}$ ($1 \le f(k, m, n) \le f_{\max}$). Let also $f'(k, m, n)$ denote the prediction value of the current pixel $f(k, m, n)$. The final prediction using LUTs is given by:

$$f'(k, m, n) = f'_{\min(\delta_1, \delta_2, \delta_3, \delta_4)}(k, m, n) \tag{7}$$

where

$$\delta_1 = \arg\left(\min\left\{\left|L_1^k[f(k-1, m, n)] - P_{ref}\right|\right\}\right) \tag{8}$$

$$\delta_2 = \arg\left(\min\left\{\left|L_2^k[f(k-1, m, n)] - P_{ref}\right|\right\}\right) \tag{9}$$

$$\delta_3 = \arg\left(\min\left\{\left|L_3^k[f(k_{final}, m, n)] - P_{ref}\right|\right\}\right) \tag{10}$$

$$\delta_4 = \arg\left(\min\left\{\left|L_4^k[f(k_{final}, m, n)] - P_{ref}\right|\right\}\right) \tag{11}$$

After the final prediction value has been produced according to (6), the set of two LUTs is updated as follows:

$$L_4^{(K)}\left[f(k_{final}, m, n)\right] = L_3^{(K)}\left[f(k_{final}, m, n)\right] \tag{12}$$

$$L_2^{(K)}\left[f(k-1, m, n)\right] = L_1^{(K)}\left[f(k-1, m, n)\right] \tag{13}$$

$$L_3^{(K)}\left[f(k_{final}, m, n)\right] = f(k, m, n) \tag{14}$$

$$L_1^{(K)}\left[f(k-1, m, n)\right] = f(k, m, n) \tag{15}$$

Figure 6 shows how two LUTs for each of the previous and final bands are utilized and updated. All LUTs are initialized with the $f_{\max}$ value that is outside the range of the data. At the decoder, the set of four LUTs and the reference prediction to decode the current pixel value are calculated from the previous and final decoded band lossless data, by following the same procedure as at the encoder.

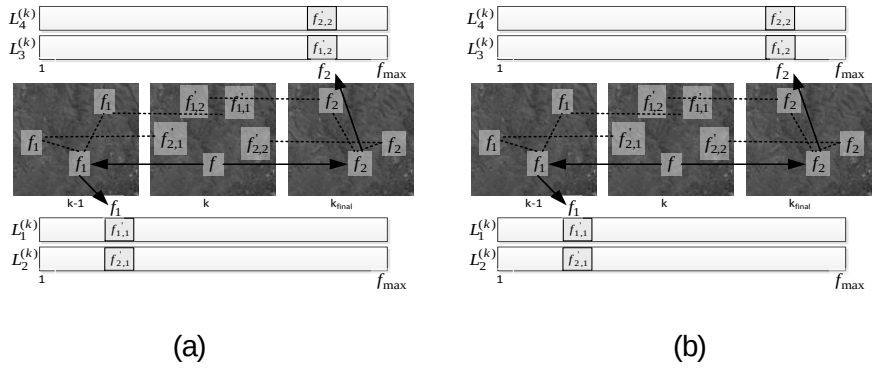

Figure 6. (a) Prediction, (b) Update Steps of the Proposed Method

Finally, by adding an additional BDPS scheme, IP3-BDPS-BPSAST and IP3-BPSAST-BDPS methods are formed. Experiments show that except for IP3-BPSAST-BDPS, the IP3-BDPS-BPSAST method can achieve some improvement for prediction.

6. Proposed Lossless Compression Method and Experimental Results

6.1. Proposed Method

Now, we depict that block diagram of the proposed lossless compression system in Figure 7. It consists of a three-stage predictor followed by adaptive arithmetic coding. The first stage attempts to decorelate the high correlated bands so that the redundancy is removed as much as possible. The second and third stages are designed to exploit the calibration-induced data correlation. The first stage operates in two modes: intraband (JPEG-LS) or interband (IP3). Once the prediction is obtained from the first stage prediction, the prediction is treated as a prediction reference, and the BDPS scheme as the second stage is applied. In the third stage, the prediction obtained from the second stage is still treated as a prediction reference, and the BPSAST scheme is employed for the final prediction.

After prediction, we use an arithmetic coding approach that is effective at encoding a source with an arbitrary distribution. Specifically, for each spectral band, we apply a separate instance of the adaptive arithmetic coder [17] of using the publicly available software implementation (http://www.cs.mu.oz.au/~alistair/arith_coder/). We use the software's adaptive zero-order integer-based model encoding method, setting all parameters to their default values.

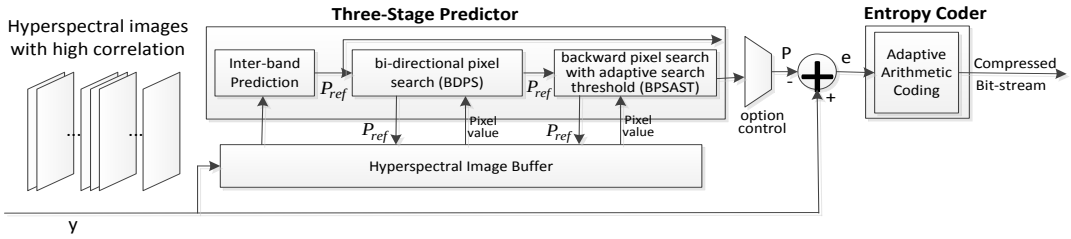

Figure 7. Block Diagram of the Proposed Lossless Hyperspectral Image Compression Method

6.2. Compression Results

In order to test the performance of our proposed algorithm, some experiments are carried out. The hyperspectral images for test are the standard AVIRIS 1997 hyperspectral images. AVIRIS covers the solar-reflected portion of the electromagnetic spectrum: 0.41-2.45 um in 10-nm bands. The AVIRIS instrument consists of four spectrometers that view a 20-m2 spot on the ground from a flight altitude of 20 km. This spot is simultaneously viewed in all the spectral bands. A spatial image is formed by moving the spectrometers perpendicular to the direction of the aircraft. The images are taken from four areas: Jasper Ridge, Lunar Lake, Cuprite and Moffett Field. The spatial size of the images is 614×512, and they contain 224 bands (these data are publicly available on the AVIRIS website at www.aviris.jpl.nasa.gov).

First, we experiment with sequence-specific threshold values for compressing all hyperspectral images. Table 1 shows the results of changing the sequence threshold values. Columns 1-4 show compression results using IP3-BDPS-BPSAST. The final row shows the average values. The results are fairly stable with regard to the sequence-specific threshold values. That indicates that we can expect the method to perform well on novel data.

Table 1. Compression Results using Sequence-Specific Threshold Values for Compressing all Hyperspectral Images (in Bits Per Pixel)

Cuprite	Jasper Ridge	Lunar Lake	Moffett Field	Average
3.67	3.99	3.68	4.00	3.84
3.71	4.03	3.75	4.05	3.89
3.66	4.00	3.70	4.01	3.84
3.69	4.02	3.72	4.03	3.87
3.68	4.01	3.71	4.02	3.86

Table 2 depicts the compression results in bits per pixel for various different compression methods for calibrated images of the AVIRIS'97 image set. Individual bit-rate values for SLSQ-OPT, C-DPCM, LUT, LAIS-LUT, LAIS-QLUT, and TSP-W2 are from [7]. Results for S-RLP, S-FMP, S-RLP-LUT, and S-FMP-LUT are from [14]. Results for 3D-CALIC, M-CALIC and IP3-BPS are from [15]. The average bit rates for four 16-bit calibrated images are shown in the last column of Table 1. The fact is that IP3-BDPS-BPSAST has the lowest bit rates. In the experiments, IP3-BDPS-BPSAST works very well on the following two images: Lunar Lake and Cuprite.

Table 2. Bit Rates (in Bits per Pixel) Achieved by Various Algorithms for Lossless Compression on the Complete AVIRIS Images

Algorithm	Cuprite	Jasper Ridge	Lunar Lake	Moffett Field	Average
3D-CALIC	5.23	5.19	5.18	4.92	5.13
R-ABPCNEF	4.94	5.03	5.06	-	5.01
SLSQ-OPT	4.94	4.96	4.95	4.99	4.96
LUT	4.65	4.95	4.71	5.05	4.84
M-CALIC	4.89	4.97	4.80	4.65	4.83
C-DPCM	4.68	4.62	4.75	4.62	4.67
S-RLP	4.69	4.65	4.69	4.67	4.67
S-FMP	4.66	4.63	4.66	4.63	4.64
LAIS-LUT	4.47	4.68	4.53	4.76	4.61
LAIS-QLUT	4.29	4.61	4.34	4.62	4.46
S-RLP-LUT	3.92	4.05	3.95	4.09	4.00
S-FMP-LUT	3.89	4.03	3.92	4.05	3.97
TSP-W2	3.77	4.08	3.81	4.12	3.95
IP3-BPS	3.76	4.06	3.79	4.06	3.92
IP3-BDPS-	3.68	3.99	3.71	4.00	3.86

In Table 3, the ratio between the IP3-BDPS-BPSAST and IP3-BPS bit rates is shown in column 5. IP3-BDPS-BPSAST shows 2% average improvement over IP3-BPS on the four 16-bit calibrated images. Similarly, the last column compares IP3-BDPS-BPSAST to LAIS-LUT. The average bit-rate improvement of IP3-BDPS-BPSAST over LAIS-LUT is 17% on the four 16-bit calibrated images.

Table 3. Compression Results for the Complete AVIRIS Images in Bits Per Pixel and Bit-Ratios Compared to IP3-BDPS-BPS

Image	IP3-BPS	IP3-BDPS -BPSAST	LAIS-LUT	IP3-BDPS-BPSAST/ IP3-BPS	IP3-BDPS-BPSAST/ LAIS-LUT
Cuprite	3.76	3.71	4.47	0.98	0.82
Jasper Ridge	4.06	4.00	4.68	0.98	0.85
Lunar Lake	3.79	3.73	4.53	0.98	0.82
Moffett Field	4.06	4.01	4.76	0.98	0.84
Average	3.92	3.86	4.61	0.98	0.83

The IP3-BDPS-BPSAST method is asymmetric with respect to computational time. Comparison between compression times between IP3-BPS and IP3-BDPS-BPSAST can be seen in Table 4. The decrease in processing time for the compression phase using IP3-BDPS-BPSAST compared to IP3-BPS is 3%. Profiling the IP3-BDPS-BPSAST method reveals that the average processing time lies in the IP3 prediction function (about 1011s), the bi-directional pixel search (about 20s), the backward pixel search with adaptive search threshold (about 326s) which is 61s less than the backward pixel search. Figure 8 shows the Adaptive search threshold and band scaling factor for the Cuprite image. The value of adaptive search

threshold is bigger than that of band scaling factor, except for Cuprite image's bands 1, 3, 7 and 111. This is also substantiated by the fact that IP3-BDPS-BPSAST is slightly faster than IP3-BPS.

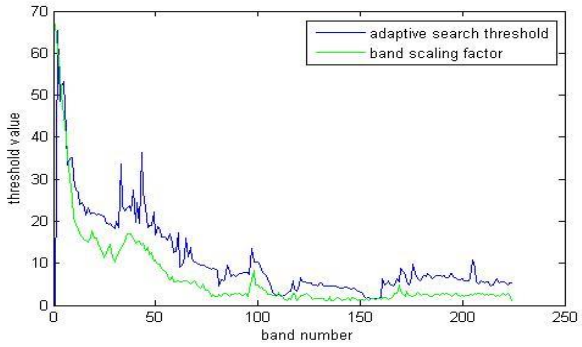

Figure 8. Adaptive Search Threshold and Band Scaling Factor for Cuprite Image

Table 4. Procession Time for the Compression Part

Image	IP3-BPS [s]	IP3-BDPS-BPSAST [s]	IP3-BDPS-BPSAST/IP3-BPS
Cuprite	1397.6	1357.4	97%
Jasper Ridge	1415.3	1370.7	97%
Lunar Lake	1437.2	1406.6	98%
Moffett Field	1408.5	1361.9	97%
Average	1414.7	1124.2	97%

As for memory usage, as we all know, the LUT method requires a full LUT for each band. Assuming 16-bit LUTs, each LUT's memory requirements are roughly equivalent to four lines of an AVIRIS image data [13]. Thus, for our test images, the amount of the memory required by LUTs is 1.1% of the memory used by the images.

7. Conclusion

We have developed an algorithm for lossless compression of hyperspectral images, called IP3-BDPS-BPSAST, which uses an efficient calibration-induced and spectral decorrelator on top of an IP3-BPS-based compression engine. Results on the AVIRIS'97 image set show that the proposed algorithm outperforms previous algorithms; a 2% increase in compression efficiency and a 3% decrease in computational complexity are observed compared to the original IP3-BPS algorithm, at the expense of a limited amount of memory resources. The proposed three-stage prediction approach should be applicable to other two-stage prediction methods such as S-FMP-LUT and S-RLP-LUT. Thus, future work includes such considerations.

Acknowledgements

This work is supported by National Natural Science Foundation of China (No. 41272363) and Youth Foundation of Sichuan Normal University (No. 10QNL05 and 09QNL09).

References

[1] X. Wu and N. D. Memon, "Context-based lossless interband compression extending CALIC", IEEE Transactions on Image Process, vol. 9, no. 6, **(2000)**, pp. 994-1001.
[2] E. Magli, G. Olmo and E. Quacchio, "Optimized onboard lossless and near-lossless compression of hyperspectral data using CALIC", IEEE Geoscience and Remote Sensing Letters, vol. 1, no. 1, **(2004)**, pp. 21-25.
[3] X. Wu and N. D. Memon, "Context-based, adaptive, lossless image coding", IEEE Transactions on Communications, vol. 45, no. 4, **(1997)**, pp. 437-444.
[4] S. Tate, "Band ordering in lossless compression of multispectral images", IEEE Transactions on Computers, vol. 46, no. 4, **(1997)**, pp. 477-483.
[5] J. Zhang and G. Liu, "An efficient reordering prediction-based lossless compression algorithm for hyperspectral images", IEEE Geoscience and Remote Sensing Letters, vol. 4, no. 2, **(2007)**, pp. 283-287.
[6] F. Rizzo, B. Carpentieri, G. Motta and J. Storer, "Low-complexity lossless compression of hyperspectral imagery via linear prediction", IEEE Signal Processing Letters, vol. 12, no. 2, **(2005)**, pp. 138-141.
[7] A. Kiely and M. Klimesh, "Expliting calibration-induced artifacts in lossless compression of hyperspectral imagery", IEEE Transactions on Geoscience and Remote Sensing, vol. 47, no. 8, **(2009)**, pp. 2672-2678.
[8] B. Aiazzi, L. Alparone and S. Baronti, "Near-lossless compression of 3-D optical data", IEEE Transactions on Geoscience and Remote Sensing, vol. 39, no. 11, **(2001)**, pp. 2547-2557.
[9] B. Aiazzi, L. Alparone, S. Baronti and C. Lastri, "Crisp and fuzzy adaptive spectral predictions for lossless and near-lossless compression of hyperspectral imagery", IEEE Geoscience and Remote Sensing Letters, vol. 4, no. 4, **(2007)**, pp. 532-536.
[10] J. Mielikainen and P. Toivanen, "Clustered DPCM for the lossless compression of hyperspectral images", IEEE Transactions on Geoscience and Remote Sensing, vol. 41, no. 12, **(2003)**, pp. 2943-2946.
[11] J. Mielikainen, "Lossless compression of hyperspectral images using lookup tables", IEEE Signal Processing Letters, vol. 13, no. 3, **(2006)**, pp. 157-160.
[12] B. Huang and Y. Sriraja, "Lossless compression of hyperspectral imagery via lookup tables with predictor selection", SPIE Proceedings, vol. 6365, **(2006)**, pp. 63650L.1-63650L.8.
[13] J. Mielikainen and P. Toivanen, "Lossless compression of hyperspectral images using a quantized index to lookup tables", IEEE Geoscience and Remote Sensing Letters, vol. 5, no. 3, **(2008)**, pp. 474-478.
[14] B. Aizazzi, S. Baronti and L. Alparone, "Lossless compression of hyperspectral images using multiband lookup tables", IEEE Signal Processing Letters, vol. 16, no. 6, **(2009)**, pp. 481-484.
[15] C.-C. Lin and Y.-T. Hwang, "An efficient lossless compression scheme for hyperspectral images using two-stage prediction", IEEE Geoscience and Remote Sensing Letters, vol. 7, no. 3, **(2010)**, pp. 558-562.
[16] M. J. Weinberger, G. Seroussi, and G. Sapiro, "LOCO-I: A low complexity, context-based, lossless image compression algorithm", Proceedings of the Data Compression Conference, Snowbird, UT, **(1996)** March 31- April 3.
[17] A. Moffat, R. Neal and I. H. Witten, "Arithmetic coding revisited," ACM Transactions on Information Systems, vol. 16, no. 2, **(1998)**, pp. 256-294.

